Controls on metal enrichment in ferromanganese crusts: Temporal changes in oceanic metal flux or phosphatisation?

Pierre Josso [a,*], Paul Lusty [a], Simon Chenery [a], Bramley Murton [b]

[a] *British Geological Survey, Environmental Science Centre, Keyworth, Nottingham NG12 5GG, United Kingdom*
[b] *National Oceanography Centre, Waterfront Campus, European Way, Southampton SO14 3ZH, United Kingdom*

Abstract

Oceanic hydrogenetic ferromanganese (Fe-Mn) crusts are a major repository for many metals, such as Co, Ni, Cu, Pt, Te and REE, which are essential for decarbonisation of transport and energy systems. Secondary mineralisation processes, occurring during phosphatisation episodes, commonly impregnate the shallower deposits with carbonate fluorapatite (CFA). The suboxic oceanic conditions during such events are frequently invoked to explain the lower Co content and unusually high Ni, Cu, Zn and Pt content of older phosphatised crusts. Here, the hypothesis of suboxic diagenetic recrystallization induced by phosphatisation episodes as a driving mechanism for Ni, Cu, Zn and Pt enrichment and Co depletion is evaluated. Accurately dated geochemical profiles, spanning 75 Ma of depositional history, for a shallow (1100 mbsl) phosphatised sample and a deeper (3100 mbsl) unphosphatised sample from Tropic Seamount in the north-east Atlantic, are compared. An isocon analysis, which allows to quantitively evaluate chemical gains and losses in mass transfer and therefore permits compensation for the dilution effect induced by the addition of CFA in the Fe-Mn crusts, demonstrates that no loss of Co has occurred in the phosphatised crust, whilst Pt, Te, Cu, Ni and Zn are enriched relative to younger, unphosphatised Fe-Mn crust. Both geochemical profiles show sympathetic trends and similar amplitudes of variation in concentration. This excludes phosphatisation as the driving mechanism for the metal enrichment and depletion. Systematic differences in metal content between the two samples, such as higher Cu and lower Co content in the deeper sample, are consistent with the depth profile of dissolved metal concentrations in the water column. The variability observed in the geochemical profiles is consistent with temporal changes in metal fluxes to the ocean, as a result of the evolving climate and oceanographic configuration of the north-east Atlantic Ocean through the Cenozoic. It is concluded that changing metal fluxes, rather than secondary mineralisation process associated with phosphatisation, is the dominant control on the primary metal content in Fe-Mn crust deposits at Tropic Seamount.
© 2021 Published by Elsevier Ltd.

Keywords: Fe-Mn crusts; Phosphatisation; Isocon analysis; Metal fluxes; Critical metals

1. INTRODUCTION

Deep-sea hydrogenetic ferromanganese (Fe-Mn) crusts, hereafter termed Fe-Mn crusts, form through accumulation of Fe and Mn oxides precipitating from ambient seawater on sediment-free surfaces in all oceans of the planet between 400 and 7000 mbsl (Lusty et al., 2018). Fe-Mn crusts are of particular interest because of their high concentrations in a range of metals of increasing economic importance (Mn, Co, Te, REY, Pt, Ni and Cu) (Hein et al., 2013; Lusty et al., 2018). Enrichment in these metals is attributed to the physio-chemical properties of Fe and Mn oxyhydroxides, and their extremely slow accumulation rates on the seafloor (a few mm/Ma), which provides an efficient and continuous scavenging mechanism for

dissolved metal species present in seawater allowing their incorporation in the mineral structure of X-ray amorphous Fe-Mn oxides and crystalline vernadite (Hein et al., 2000; Koschinsky and Hein, 2003).

During periods of major oceanic circulation overturning, upwelling of nutrient-rich deep waters results in rapid increases in biological productivity, resulting in oxygen depletion in the upper water column (Halbach and Puteanus, 1984). This causes the formation of a phosphate-saturated oxygen minimum zone (OMZ) extending downwards in the water column. If the summits of shallow seamounts intersect the OMZ, the suboxic seawater conditions have three potential effects on existing Fe-Mn crusts: (i) inhibiting further growth; (ii) chemical dissolution and/or diagenetic modification of Fe-Mn oxides, carbonates and biological tests; and (iii) precipitation of carbonate fluorapatite (CFA) in the pore space of the crusts and their substrates (e.g. carbonates, volcanics etc.), resulting in partial or total replacement of existing carbonates (Grant, 1986). Strong suboxic conditions can notably lead to the partial-dissolution of Fe and Mn oxyhydroxides and precipitation of more stable secondary mineral phases such as todorokite with varying metal accommodation mechanisms (Halbach et al., 1989a, 1989b; Koschinsky et al., 1997).

A number of authors have investigated the effect of suboxic conditions on existing Fe and Mn oxides, their partial dissolution pathways, fields of stability, reprecipitation into secondary diagenetic minerals such as todorokite, associated metal fixation processes, and concentrations of dissolved metals in the OMZ (Koschinsky et al., 1997; Hein et al., 2000; Jiahua et al., 2005; Mizell et al., 2020a). Notably, Koschinsky et al. (1997) conducted mixing calculations between a phosphorite and unphosphatised crust to quantify dilution effects of additional CFA. Whilst changes in the spatiotemporal fluxes of metals to the ocean have also been considered as a possible explanation for these variations, in the absence of comparative unphosphatised samples from the same location and spanning a similar period of deposition, the effect of natural stratigraphic geochemical variations could not be properly evaluated and geochemical variations observed in phosphatised samples have been dominantly attributed to dilution and secondary diagenetic processes.

Major phosphatisation episodes have been identified in the Pacific Ocean between 39–34 Ma (peak at 37 Ma) and 27–21 Ma (peak at 25 Ma) (Hein et al., 1993). In the north-east Atlantic, phosphatisation episodes have been accurately dated between 59–54 Ma and about 38 Ma (Josso et al., 2020b), and between 25–18 Ma (González et al., 2016). As a result, Fe-Mn crust samples from seamount summit areas commonly exhibit a dual structure, comprising older phosphatised crust overlain by younger unphosphatised Fe-Mn oxides. Geochemical analysis of Fe-Mn crusts from most oceans have consistently highlighted an enrichment in Ni, Cu, Zn, and notably Pt in phosphatised samples, and lower Co content relative to unphosphatised materials (Koschinsky et al., 1997; Hein et al., 2000). Therefore, it is generally considered that the phosphatisation process is detrimental to the Co content, the metal of greatest economic importance in Fe-Mn crusts

(Lusty et al., 2018). When considering the potential for future economic extraction of metals from Fe-Mn crust deposits, ease of access and operations, which will be influenced by water depth, seafloor topography and gradient, are of paramount importance. Accordingly, the shallow flat tops of guyots and seamounts are the most promising targets for commercial extraction. However, they are also most prone to post-depositional phosphatisation events.

In 2016, the MarineE-Tech project recovered more than 350 Fe-Mn crust samples from the Early Cretaceous age Tropic Seamount, in the north-east Atlantic, from between 1000 and 4000 meters below sea level (mbsl). The accurate dating of an Fe-Mn crust sample (Josso et al., 2019) and development of a Pb isotope correlated stratigraphy at the seamount-scale (Josso et al., 2020a) provide evidence that Fe-Mn crusts on the flanks (078_019, 3100 mbsl) and summit of Tropic Seamount (085_004, 1100 mbsl) represent a depositional period spanning the last 75 Ma. Detailed investigation of the mineralogy and texture of the summit sample identified two major phosphatisation events, the first at the Paleocene – Eocene transition and the second at 38 Ma ago, which impregnated the lower half of the sample with CFA (Josso et al., 2020b). There is no evidence of phosphatisation in the deeper sample 078_019.

This study provides a comparison of accurately dated geochemical profiles for two Fe-Mn crust samples recovered at 1100 and 3000 mbsl on Tropic Seamount. Preservation of the 75–28 Ma period of deposition in both samples provides an opportunity to compare the geochemistry of contemporaneous Fe-Mn crusts layers and evaluate the effects of diagenetic phosphatisation on the metal contents of the summit sample. When comparing the differences in metal content between the samples, changes in sample depth over time as a function of seamount subsidence and sea level changes are considered. An isocon analysis, a robust method widely employed to explore element gains and losses during hydrothermal alteration of a protolith (Grant, 1986), is applied in this study. This represents the first time this technique has been applied to Fe-Mn crusts to assess the influence of diagenetic phosphatisation and mass changes on their element's budgets.

2. MATERIAL AND METHODS

2.1. Fe-Mn crust samples

During 2016 a UK-led research expedition on the RRS James Cook (JC142) visited Tropic Seamount, as part of the MarineE-Tech project. The seamount is situated 450 km off the coast of West Africa and is part of the Saharan Seamount Chain. Summit sample 085_004 was recovered using an ROV-mounted drill from an Fe-Mn crust pavement at 1130 mbsl located on the flat top area of the seamount. This core preserves 15 cm of Fe-Mn crust on a phosphatised carbonate substrate (Fig. 1). A detailed age model was established for this sample by integrating Os isotope (n = 53), laser-ablation ICP-MS U-Pb (n = 60) and Co-chronometry (n = 123) data using statistical modelling (Josso et al., 2019). Josso et al. (2020b) presented a detailed investigation of the geochemistry and textures of the core
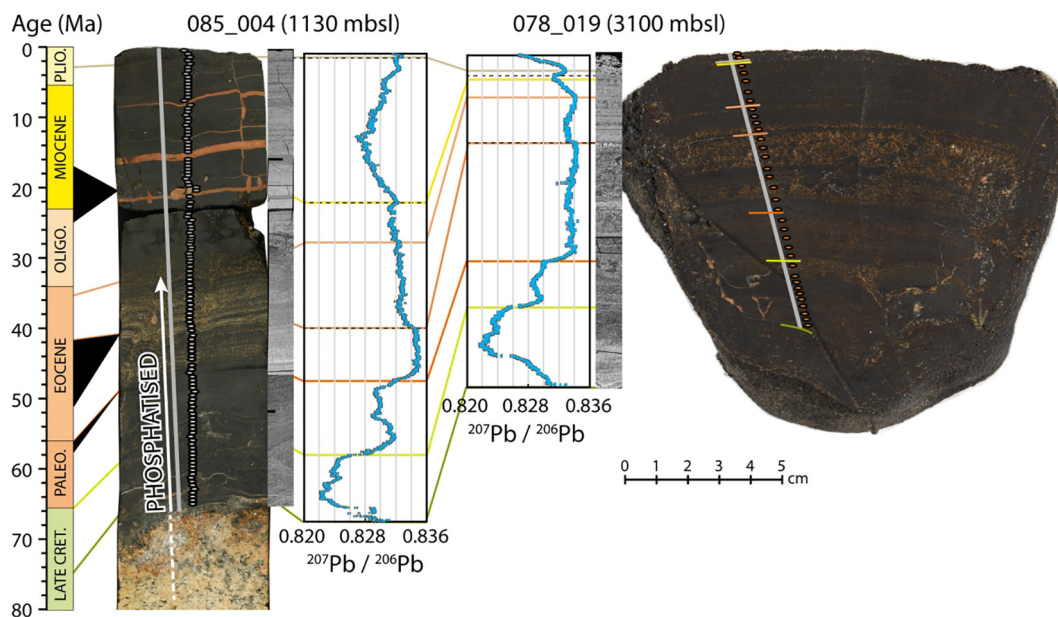
Fig. 1. Age correlation between the summit sample 085_004 and the flank sample 078_019. The initial age model was established on 085_004 (Josso et al., 2019) and transposed to other samples from Tropic Seamounts, based on their Pb isotopes profiles (Josso et al., 2020a). Horizontal lines represent Pb isotope fix points at 75, 66, 56, 42, 17, and 3 Ma respectively from bottom to top, whilst black triangle are hiatuses (Josso et al., 2019). Stratigraphic SEM backscatter profiles were produced for both samples and detailed images are provided in Supplementary Material 1. The grey lines overlain on both samples represent the laser ablation profile, the white line shows the extent of the summit sample that is phosphatised, and the dots indicate the stratigraphic layer subsampled by hand-held micro-drill.

for the purpose of paleoceanographic interpretations. The flank sample 078_019 was recovered from the western spur (3100 mbsl) of Tropic Seamount, using a ROV manipulator arm. When cut, the boulder-like sample has no visible substrate. A 2 cm thick, relatively recently formed rim of Fe-Mn oxide layers, englobes the rest of the sample (Fig. 1). This suggests it was overturned by a local destabilising event affecting the flank of the seamount. Whilst this may mean the sample originally formed at a shallower water depth, evidence provided by Nd isotopes demonstrate that these two samples record the signature of different water masses until the Eocene-Oligocene transition, before progressive shoaling of the deep-water mass subsequently bathing both samples in Northern Component Water (see Josso et al. (2020a) for detailed discussion). Furthermore, the absence of CFA is additional evidence that flank sample 078_019 was forming sufficiently deep to not be affected by the phosphatisation episodes. Finally, geochemical data presented in the results indicate a consistent difference in water depth of the two samples throughout their depositional history.

2.2. Temporal framework

The age model for summit sample 085_004 was transposed onto sample 078_019 by correlating their Pb isotope trends, as described in Josso et al. (2020a) and summarised in Fig. 1. Both samples contain Fe-Mn oxides deposited during the following periods: 75–52 Ma, 41–28 Ma, and most recently at 2 Ma. Sample 085_004 additionally preserves the 16–2 Ma portion of the record, which is absent

in the flank sample (078_019) and is assumed to have been eroded.

2.3. Geochemistry

Between 0.03 and 0.16 g of micro drilled sample (0.1 g of reference materials) weighed into PFA vials were first pre-digested in a mixture of concentrated nitric and hydrochloric acid to solubilise the main oxide/hydroxide and phosphate components at 80 °C until dry. The residue was subjected to a mixed acid attack of nitric, hydrofluoric and perchloric acids by heating over-night in a step heating programme from 80 °C to 160 °C using a programmable hot-block to ensure dissolution of silicates (Josso et al., 2020b).

Samples were analysed using an Agilent 8900 ICP-MS using He collision cell gas mode to minimise risk of spectral interferences for all elements except As and P, analysed in O_2 gas mode, for best detection limits and interference removal. Calibrations and quality control were made using a series of dilutions of a custom multi-element solution blend from QMX, UK. Residual interferences such as LREE oxides on HREE were corrected for using single element interference solutions. Individual samples were diluted according to mass to ensure best detection limits while ensuring they were within calibration ranges. Whole procedure QC was conducted by means of digestion blanks and reference materials. Three reference materials (Nod-A-1, Nod-P-1, and JMn-1, see reference values in Jochum et al. (2005)) and one in-house material (HRM) were digested and analysed in triplicate. The precision (repeata-

bility) for all elements, significantly away from their detection limit, was better than 5%. The complete geochemical dataset is available for download from the National Geoscience Data Centre (https://doi.org/10.5285/a2a0347b-530a-4798-83d2-61eb3cce78fe).

2.4. Isocon analysis

Element fluxes in the phosphatised samples were investigated using the immobility isocon diagram method (Gresens, 1967; Grant, 1986). This approach predicts that elements identified as immobile during an alteration or mineralisation event, can be used to estimate gains and losses of other components (Gresens, 1967; Humphris et al., 1998).

Immobile elements in Fe-Mn crust subsamples were identified using 2D plots for all unphosphatised and phosphatised subsamples from summit sample 085_004. To be considered immobile, elements are required to define a straight line passing by the origin of the plot with significant positive correlation. Therefore, the ratio for any two elements must remain constant between phosphatised and unphosphatised samples for them to be considered immobile. This follows the logic that immobile element content will either be diluted by mass gain (addition of CFA), becoming closer to the origin as infinite dilution ultimately decreases the concentration to zero, or increases if mass is removed during alteration or mineralisation events.

Whilst a single immobile element is sufficient to calculate mass balance, immobility in intense alteration zones could result from a variety of processes, such as the nature of the protolith and its heterogeneity, analytical errors and departure from the ideal element immobility. To minimize inherent errors as a result of these factors, determination of the isochemical line, or line of no-mass transfer, must be based on as many species as possible, even if this results in some scatter and increases the uncertainty in the quantification of mass gains and losses (Grant, 1986). Element pairs with a strong correlation in both unphosphatised and phosphatised principal component analysis (Supplementary Material 2) were considered and their ratio used for correction (see Supplementary Material 3 for details on calculation of the isocon method).

3. RESULTS

The variations in texture, mineralogy and major element geochemistry of summit sample 085_004 are discussed by Josso et al. (2020b) in the context of their importance to paleoceanographic reconstructions. This previous study, and a number of others (Koschinsky et al., 1996; Marino et al., 2017), indicate that the Fe-Mn crust samples from Tropic Seamount are hydrogenetic, with average compositions typical of Fe-Mn crusts occurring proximal to continental margins. Paleo reconstruction of the subsidence of Tropic Seamount over the last 150 Ma (Supplementary Material 4) demonstrates that there were negligible bathymetric variations over the period of Fe-Mn crust deposition (Crosby and McKenzie, 2009; Dutkiewicz et al., 2015; Frank and Arthur, 1999; Haq, 2014; Haq et al., 1987; Tripati et al., 2005; Watts and Zhong, 2000; Yeo et al.,

2018). Both samples formed in a relatively narrow depth window, varying by only about 300 meters (Supplementary material 4). Significant changes in water depth over the last 75 Ma can, therefore, be excluded as a major influence on the stratigraphic variation in metal concentrations in the Fe-Mn crusts at Tropic Seamount.

The summit sample is dominated by X-ray amorphous Fe and Mn oxides and goethite, with minor quartz and Mg-rich calcite, and abundant carbonate fluorapatite in its lower phosphatised portion (Josso et al., 2020b). Two subsets of subsamples, based on the phosphorus content are distinguished for the summit sample: phosphatised (n = 61) and unphosphatised (n = 62), and discussed separately below.

3.1. Metal content

The concentration of transition and precious metals in Tropic Seamount crusts (https://doi.org/10.5285/a2a0347b-530a-4798-83d2-61eb3cce78fe) are presented in Fig. 2, alongside regional means for the global ocean (Hein et al., 2013). The spread of geochemical data shown by the flank sample and the phosphatised and unphosphatised sample subsets from the summit sample span the range of regional mean metal values for Fe-Mn crusts in the world's oceans, most notably for Co, Zn and Pt. Large differences in Cu (five-fold) and Co content between the flank and summit samples relate to the water depth that the crusts formed at. The Ni concentrations of all subsets are consistent with Atlantic, Indian and non-prime Pacific Ocean regions, at about 0.2 wt% below concentrations found in the Pacific prime-crust zone (PPCZ). Relative to regional means, the Te content of Tropic samples is amongst the highest reported in the literature (50–250 ppm). Marino et al. (2017) report mean platinum value of 182 ppb for Tropic Seamount, which is consistent with platinum concentrations reported for the unphosphatised summit sample in this study. In contrast, platinum values are on average twice as high in the phosphatised subset and the flank sample from Tropic Seamount (100–900 ppb, Fig. 2).

The total REE and Y (REY) content is statistically similar (p-value = 0.75 in test of similarity) in both the phosphatised and unphosphatised subsamples (085_004) and flank (078_019) samples (mean 0.29 ± 0.08 wt.%, 0.24 ± 0.13 wt.% and 0.28 ± 0.10 wt.%, respectively). Post-Archean Australian shale (PAAS, Taylor et al. (1985)) normalised (SN) trends exhibit signatures typical of hydrogenetic precipitation, with subchondritic Y_{SN}/Ho_{SN} ratios and positive Ce and negative Y anomalies (Fig. 3). The phosphatised subsamples are distinct in their higher La_{SN}/Sm_{SN} and Y_{SN}/Ho_{SN} ratios and lower Gd_{SN}/Yb_{SN} ratios reflecting the stronger seawater-like signature of CFA (Fig. 3C & D). Beyond the dilution effect of CFA precipitation, these characteristics of the phosphatised subsamples (Fig. 3B) were interpreted to reflect a minor diagenetic influences, or less suboxic conditions of the phosphatisation episodes, compared with the phosphatised samples from the Pacific Ocean exhibiting strong positive Y anomalies and Y/Ho ratios above chondritic values despite
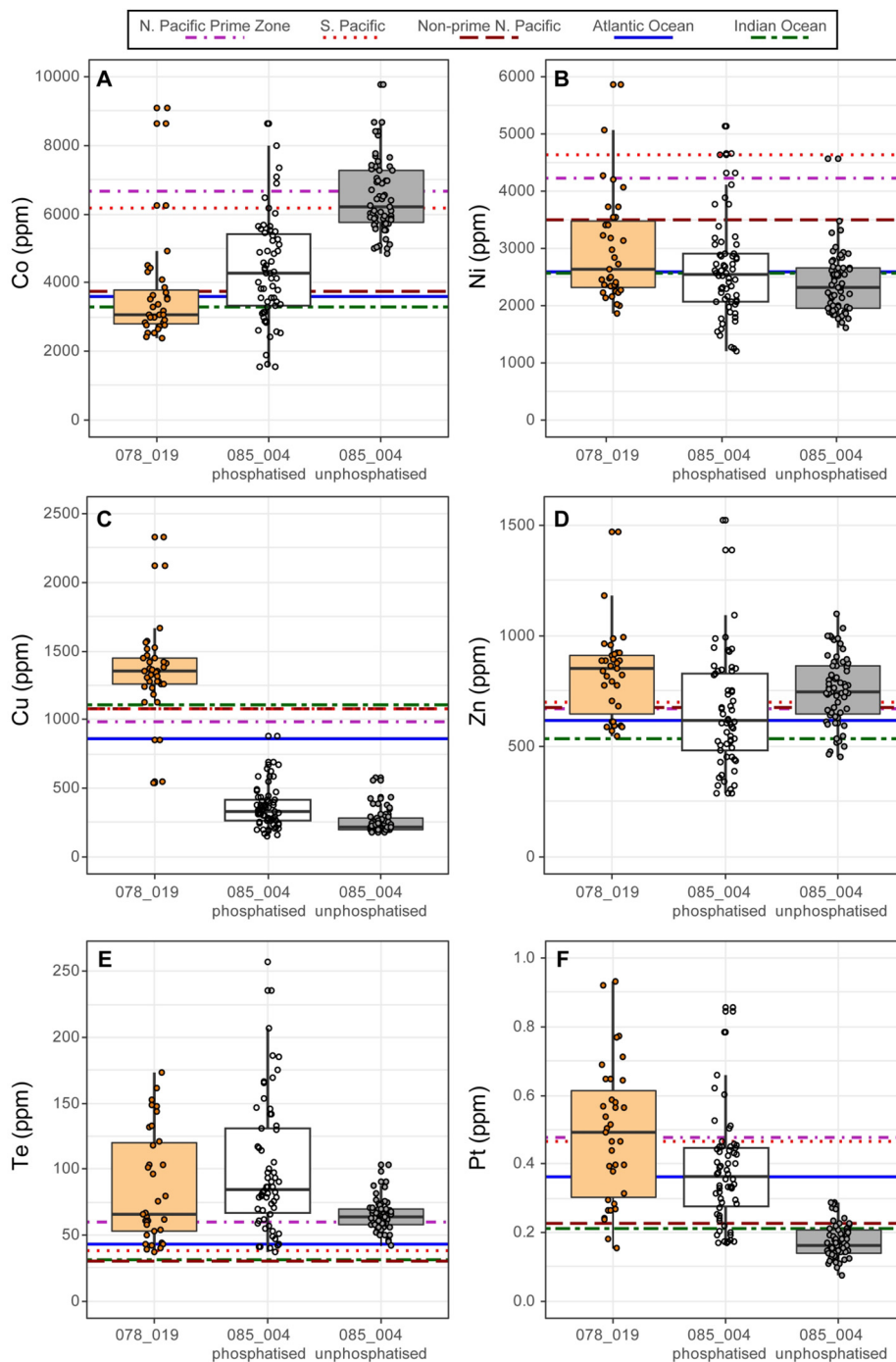
Fig. 2. Box and whisker plots for Co, Ni, Cu, Zn, Te and Pt for the flank sample 078_019 (3100 mbsl), and the phosphatised and non-phosphatised subsets of summit sample 085_004 (1100 mbsl). The coloured horizontal lines represent regional means reported by Hein et al. (2013). Note that the average Pt value for the Atlantic Ocean includes data from Muiños et al. (2013) to complement the only two bulk values reported in Hein et al. (2013). The complete dataset is available at https://doi.org/10.5285/a2a0347b-530a-4798-83d2-61eb3cce78fe.

comparable P content (1.6–4.4 wt.%) (Bau et al., 1996; Josso et al., 2020b). Primary content of biogenic carbonates and porosity dictated by mineral textures play a large role in controlling the measured Ca and P content which does not relate to the intensity or duration of suboxic conditions. These distinct Y anomalies and Y/Ho ratios might relate to

the difference in oceanographic setting between Pacific Ocean seamounts and the continental margin context of Tropic Seamount (Bau et al., 1996; Hein et al., 2016). It is likely that the more pronounced upwelling on the eastern side of the Atlantic basin minimised the impact of phosphatisation.
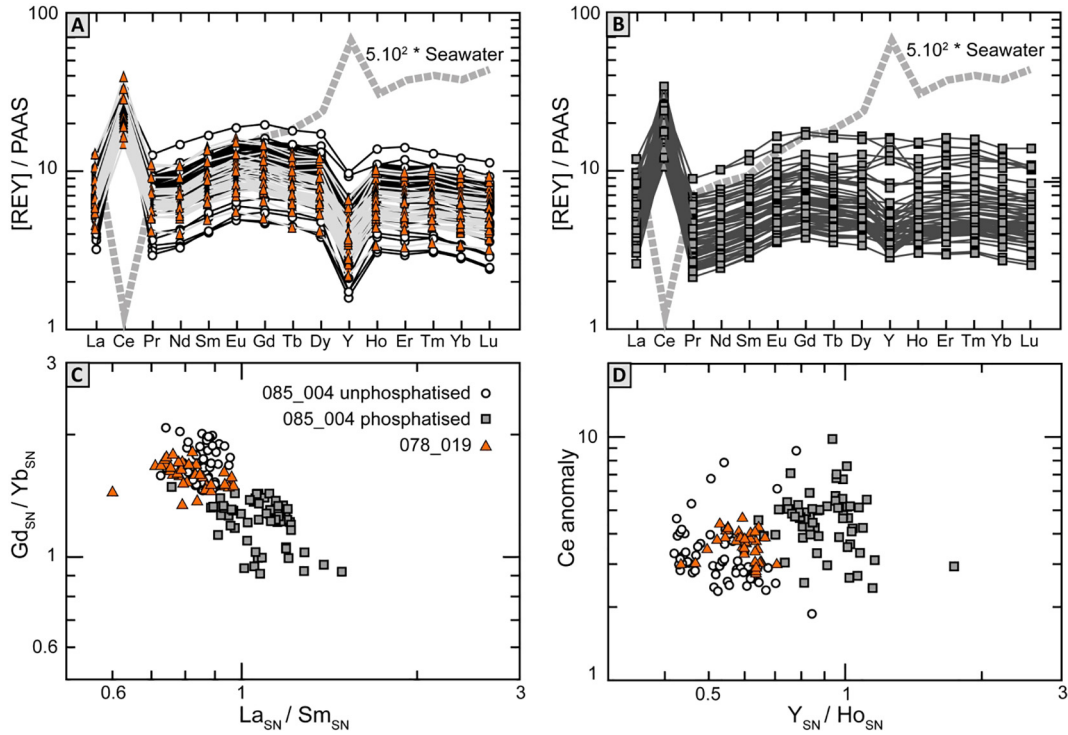
Fig. 3. PAAS-normalised (Taylor and McLennan, 1985) REE and Y compositions. (A) unphosphatised subsamples from samples 085_004 and 078_019. (B) Phosphatised subsamples from sample 085_004. Major differences in trends are highlighted by distinct populations in the following plots: (C) Gd$_{SN}$/Yb$_{SN}$ vs. La$_{SN}$/Sm$_{SN}$ ratios and (D) the Ce anomaly vs. Y$_{SN}$/Ho$_{SN}$ ratios (modified from Josso et al. (2020b)).

3.2. Comparison of phosphatised and unphosphatised composition

Many authors (Halbach and Puteanus, 1984; Halbach et al., 1989a; Halbach et al., 1989b; Koschinsky et al., 1997; Hein et al., 2000; Jeong et al., 2000; Jiahua et al., 2005; Asavin et al., 2010; Hein et al., 2013; Marino et al., 2017; Benites et al., 2020) have compared the bulk element composition of phosphatised and unphosphatised crust samples. It is generally observed that phosphatisation causes enrichment in Ni, Cu, Zn, Ba, Sr, Pt, Ce, Te, HREE, Y, Cr, and Ba, and depletion in Si, Fe, Al, Ti, Co, Mn, Zr, Th, U, Pb.

The normalised mean composition of the phosphatised sample subset from the summit sample 084_004, relative to the unphosphatised sample subset (Fig. 4) is consistent with this general pattern. Although the effect of dilution by CFA is acknowledged in some previous studies, it is rarely quantified or corrected for. Calculations from Koschinsky et al. (1997) constitute one of the most robust attempts at comparing metal content in unphosphatised and phosphatised crusts using compositional endmember mixing calculations between a phosphorite (phosphatised limestone) and an unphosphatised crust. The remaining discrepancies between their calculations and the measured phosphatised crust composition were attributed to addi-
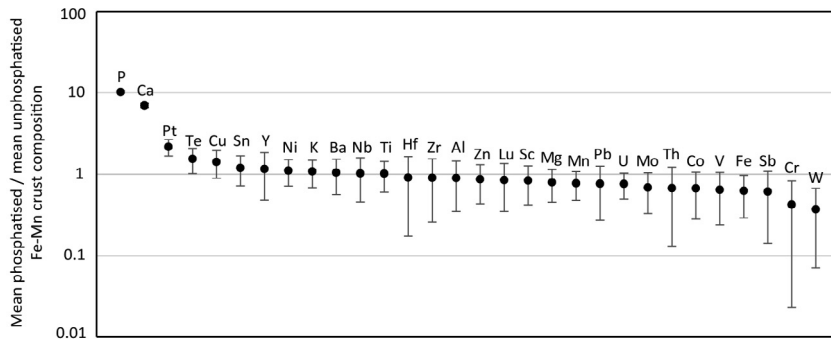

Fig. 4. Mean composition (±2σ) of the phosphatised subsample set normalised to the mean of the unphosphatised subsample set from sample 085_004.

tional suboxic diagenetic effects and precipitation of metals together with the CFA (Koschinsky et al., 1997). A different approach is proposed here with the use of an isocon diagram to understand element gains and losses between a pristine protolith and an altered or mineralised rock, accounting for mass changes, such as addition of CFA in the Fe-Mn crust system.

Based on the Pearson coefficient correlation matrices (Supplementary Material 2), all element pairs showing strong correlations in both the phosphatised and unphosphatised subsets of summit sample 085_004, were assessed for immobile behaviour (Fig. 5).

Vanadium, Fe and Sb demonstrate the closest characteristics to immobile behaviour in the dataset with regression lines of similar slopes and intercepts, low data scatter and high correlation values. These three elements have similar mass change term ($C_{unphosphatised}/C_{phosphatised}$ = 1.54, 1.59, 1.62, supplementary material 3) and are therefore considered immobile under conditions of phosphatisation at Tropic Seamount. That these redox sensitive elements remained immobile and within the crust system suggests conditions were not strongly suboxic at Tropic Seamount and that phosphatisation mostly had a dilution effect, in good agreement with REE data. Other element pairs with a good correlation such as Mo-Mn and Ba-Zn have mass change terms too dissimilar to suggest immobility during phosphatisation (1.45–1.28 and 0.95–1.15, respectively), also highlighted by divergent regression lines, which might be caused by decoupled metal sources or minor metal migration during suboxic conditions. Other pairs were not con-
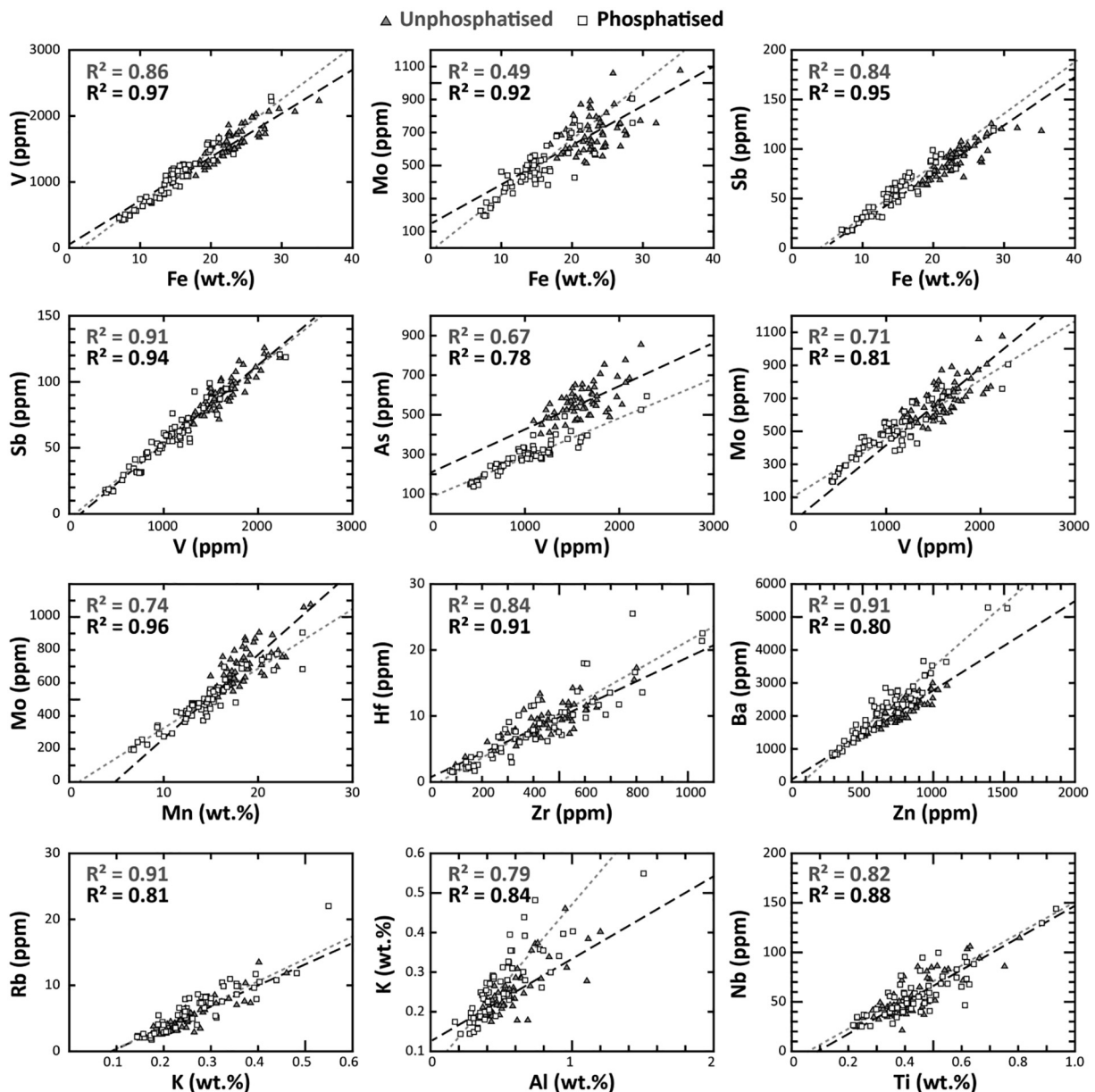

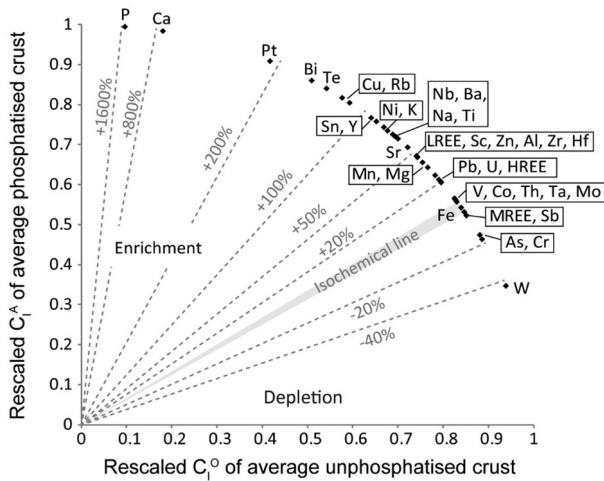Fig. 5. 2D plots for co-varying elements in both phosphatised and unphosphatised subsamples from sample 085_004.

Fig. 6. Isocon diagram for the mean composition of phosphatised subsamples (n = 61) rescaled against the mean composition of unphosphatised subsamples (n = 62) from sample 085_004. The corrected data for mass-transfer are normalised so that the sum of squares equals 1, avoiding errors in graphic interpretation due to arbitrary scaling (Humphris et al., 1998). The average mass change term from Fe, Sb and V is then used to correct for altered concentrations to calculate element gains and losses in isocon diagrams (Supplementary Material 3).

sidered due to their poor correlation coefficients, high scatter and/or regression lines not passing proximal to the origin of the diagram. Therefore, the average C_{iA} = 1.59 for V, Fe and Sb is used for correcting dilution of other elements (supplementary material 3) resulting in a precision of ±3% on reported mass gains and losses.

The isocon analysis shows a similar sequence of relative variations (Fig. 6). However, the benefit of this method is for estimating which elements define the point of reference to quantify mass gains and losses. The mean phosphatised composition (n = 61) is enriched in P and Ca, but also has a mass gain in Pt (+245%), Bi (+168%), Te (+146%), Cu (+125%), Sn (+90%), Ni (+76%), Nb (+62%), Zn (+38%), Sc (+33%), and Mn (+23%) relative to the mean unphosphatised composition of 085_004. Accounting for the effect of CFA dilution demonstrates no loss of Co in these phosphatised subsamples, since together with Mo and Ta, these elements fall within uncertainty of the array of the Fe, V, Sb isochemical line. Net element losses are observed solely for Cr (−14%), As (−17%), and W (−42%). Based on this, it can also be concluded that neither Fe nor Mn oxides suffered losses induced by the suboxic conditions of phosphatisation at Tropic Seamount.

The isocon analysis confirms the commonly observed higher concentrations of Pt, Te, Bi, Cu, Ni, and Zn in the older, phosphatised part of summit sample 085_004, and demonstrates that no cobalt was lost as a result of phosphatisation, when mass variations are accounted for.

3.3. Geochemical profiles

Here we assess whether the metal enrichments and depletions highlighted by the isocon analysis are related to diagenetic processes as exemplified by Koschinsky et al. (1997) or temporal variations in metal fluxes by comparing the geochemical profiles of the summit and flank samples (Fig. 7).

Overall, the geochemical profiles from the flank sample (078_019) are smoother and show fewer extreme values (Fig. 7). The more homogenous texture of sample 078_019; predominantly columnar throughout its stratigraphy with the exception of some more laminated intervals, contribute to smoother geochemical profiles (Fig. 1, supplementary material 1). In contrast, textural changes in 085_004 are frequent, ranging from compact laminated layers to columnar, with variable porosity filled by biogenic carbonates and CFA. This explains the variable P content of the summit sample and explains some of the significant variation (up to 3-fold) in the concentration of some other major elements, notably Fe and Mn (Figs. 1 and 7), in the Eocene section of the summit sample (Josso et al., 2020b). Unphosphatised parts of both 085_004 and 078_019, contain 0.3–0.5 wt.% P, whilst the P content increases to 2.5–8 wt.% in the phosphatised part of the summit sample. These features represent varying current energy, growth rate, and variously effect the bulk geochemistry because of dilution by biogenic and detrital material (Fig. 1, Josso et al. (2020b)). The more homogenous texture of the flank sample is consistent with the lower energy, less dynamic oceanic environment present at greater water depths. This contrasts with the higher energy, more variable conditions that prevail on the shallow, flat summit of Tropic Seamount influenced by tidal energy (Yeo et al., 2019).

Cobalt concentrations increase stratigraphically upwards in both samples; however, the flank sample has concentrations that are on average 20–40% lower than in the summit sample. Both samples have very similar stratigraphic profiles for Ni, Zn, Mo and Ba and the range of concentrations for these elements also overlap in both samples. With the exception of the two youngest subsamples, representing the 2–0 Ma section of its stratigraphy and where Cu concentrations reduce to 846 and 575 ppm, Cu has a consistent concentration in the flank sample, averaging about 1500 ppm. Copper content in 085_004 continuously decreases from about 700 ppm to 235 ppm between 75 and 10 Ma, whilst in the most recent 10 Ma section of the sample, Cu concentrations increase back to 600 ppm.

Profiles for Pt and Te from the two samples have many similarities, with high amplitude variations, of up to fivefold between 75–52 Ma. Strong enrichments in Pt in the two samples occur in the same stratigraphic intervals, notably at about 59 Ma and 55–54 Ma. However, only the summit sample is enriched in Pt at about 67 Ma. A similar pattern is apparent for peak concentrations of Te, with values twice as high as the mean at 67 Ma (only observed in the summit sample), 62 and 55–54 Ma (in both samples). Te and Pt profiles in both samples for the 41–0 Ma period are relatively constant, with less than a 2-fold amplitude variation observed. However, the average Te and Pt content is much lower (by 40–50% and 55%, respectively), than their average concentration in the 75–41 Ma section of Fe-Mn crust.
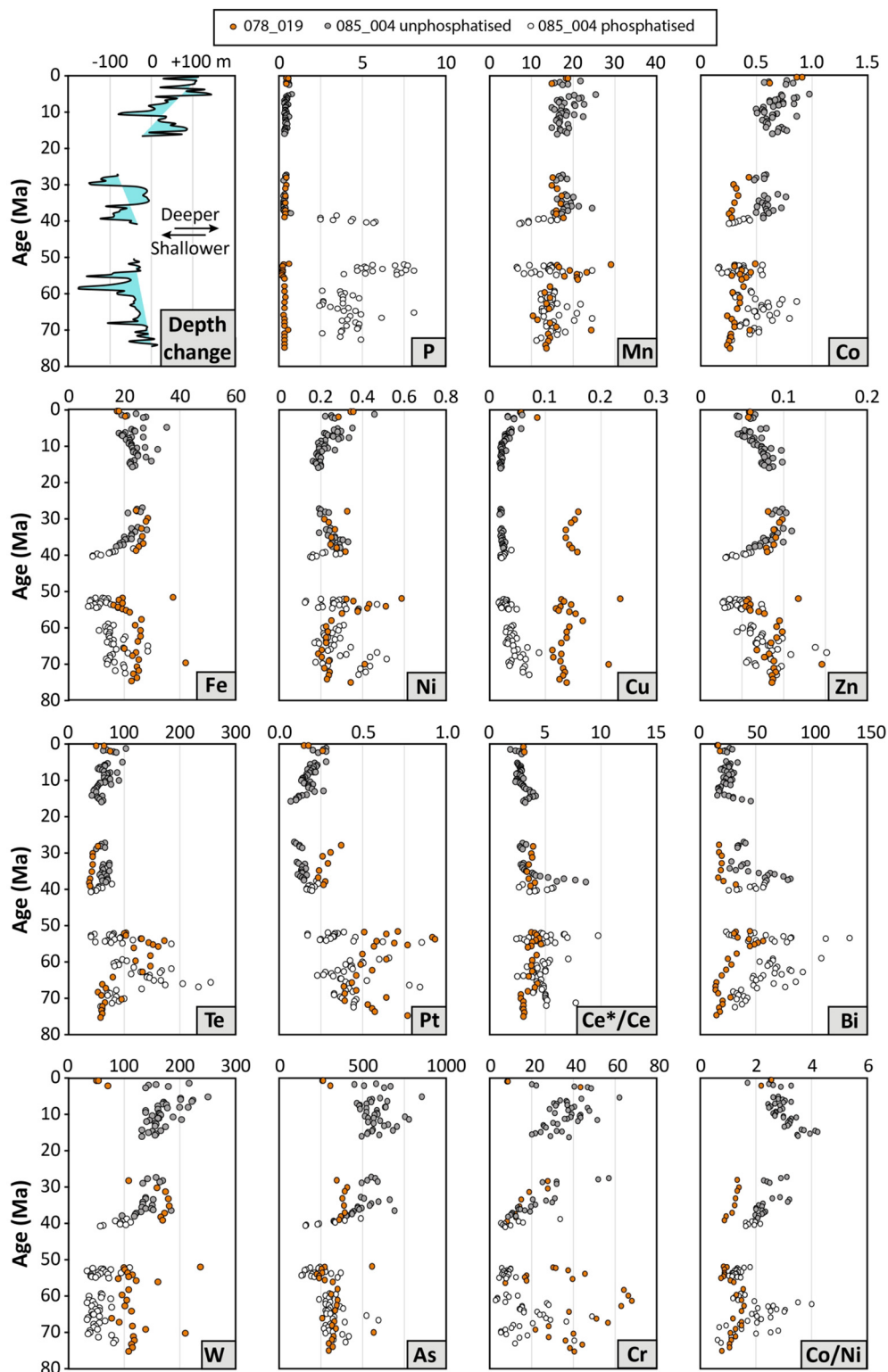
Fig. 7. Selected element profiles for sample 085_004 (summit) and 078_019 (flank). P, Mn, Co, Fe, Ni, Cu, Zn are expressed in wt.%, Te, Pt, Bi, W, As, Cr are in ppm, and Co/Ni and Ce*/Ce are dimensionless. The depth change diagram shows the relative variation for both samples from their initial depth of formation 75 Ma (Supplementary Material 4). Note that high Fe, Mn, Co, Ni, Cu, Zn, As, Mo, W, V, Sb and REY in two flank subsamples at 70 and 51 Ma correspond to intervals with high electron back-scatter intensity on the SEM stratigraphic profile from 078_019 and are proximal to an erosive surface (Supplementary Material 1).

4. DISCUSSION

The geochemical data for the two stratigraphic sections highlights some sympathetic trends, despite significant variations in total metal content between the flank and summit regions. The isocon analysis indicated higher Ni, Cu, Ni, Zn, Pt and Te content in the phosphatised subset of sample 085_004, with no losses in Fe, Mn or Co as mass changes are corrected. These observations suggest that phosphatisation is not the dominant factor controlling metal concentration in Fe-Mn crusts.

4.1. Effect of depth variations

The paleo-depth reconstruction (Supplementary Material 4, Fig. 7) shows that both samples underwent minor depth changes during their depositional history, becoming shallower by 150 m between 75–30 Ma and then becoming gradually deeper by a total of 260 m over the last 30 million years. The OMZ in the waters that currently surround Tropic Seamount contain 50 µmol kg^{-1} of dissolved O_2 at water depths between 300–700 mbsl (Schlitzer et al., 2018). Whilst unlikely similar conditions prevailed during the last 75 Ma, it is likely that the summit sample was located in or just below the OMZ for most of the period when crusts were developing. Phosphatisation of the Fe-Mn crusts on the summit during events at 59–54 Ma and 38 Ma indicates extension of the OMZ depth to at least 1010 mbsl (Supplementary Material 4). In contrast, the flank sample, located between 3080–3400 mbsl during its entire depositional history, would not have been significantly impacted by variations in the position and strength of the OMZ. It is commonly observed that a strong OMZ favours enrichment in Mn as well as in Co and Ni by association to Mn oxides, compared to locations with weak or no OMZ (Mizell et al., 2020b). As both samples come from the same seamount, the minor but significant difference in Mn over the last 40 Ma (18.4 ± 4.5 wt.% and 16.8 ± 2.6 wt.%, p-value = 0.003) is likely to reflect the effects of water depth on availability of dissolved elements from the OMZ reservoir. Most differences in element concentration between the two samples and their respective trends can be related to the profile of dissolved elements in the water column. The extensive data set on seawater properties and dissolved metal content arising from the GEO-TRACES expedition GA03_E and GA03_W, which passed close to Tropic Seamount, provides an excellent basis for discussing the current situation in this part of the northeast Atlantic (Schlitzer et al., 2018).

Recycled, or nutrient type elements (e.g. C, P, N, Si, Cu, Fe, Zr, Nb, etc.), play a major role in biological processes. As a result, these elements are depleted in surface waters and their content increases progressively with depth, carried by sinking organic matter and skeletal tests that are recycled. The Cu data from the Fe-Mn crusts presented in this study reflects the pattern in the GEOTRACES data, whereby dissolved Cu (^{dis}Cu) content increases by 75–100% between 1000 and 3000 mbsl around Tropic Seamount (Schlitzer et al., 2018). This is the reason for the large difference in the Cu content of the two samples stud-

ied here. Iron, Zr, Nb, Ta also show a similar pattern, with continuous recycling at depth. However, variation in their concentration in different parts of the water column is less (Firdaus et al., 2018). Other nutrient-type elements, such as Ni, Zn or Ba, do not show any differences in concentration between the summit and flank samples, which is consistent with only a minor (10–20%) increase in the dissolved concentrations of these elements in the GEOTRACES data between 1000–3000 mbsl.

Scavenged-type elements are abundant in surface waters and tend to decrease with depth due to their high reactivity and adsorption onto sinking particles. Cobalt is a prime example, with an 80% decrease in ^{dis}Co between 1000 and 3000 mbsl (Schlitzer et al., 2018). This is clearly reflected in the Co concentrations of the flank sample which were in bulk 20–40% lower than in the summit sample. In both samples, the similar thicknesses (44 and 40 mm for the summit and flank samples, respectively) for the well-developed stratigraphy of the 75-58 Ma period, implies a faster growth rate for the summit sample despite higher Mn and Co content. This finding highlights the impact of dissolved species availability for scavenging into Fe-Mn crusts, despite the dilution effect of varying growth rate usually considered dominant and on which Co-chronometers are relying. Similarly, Pb and Sc are scavenger-type elements, and have lower concentrations in the flank sample. Mn is traditionally considered a scavenger-type element, with maximum total Mn content typically occurring in the suboxic OMZ. In seawater Mn cycles between oxidized insoluble Mn oxides ($Mn(III/IV)O_x$) and soluble species of reduced oxidation state occurring as soluble Mn^{2+} ions or complexed to organic ligands (Mn(III)-L) (Oldham et al., 2017). However, the OMZ in the north-east Atlantic is not very pronounced, which results in ^{dis}Mn concentrations decreasing significantly from the surface to 100 mbsl and then becoming stable below 700 mbsl. This pattern of Mn distribution in the water column is consistent with higher Mn in the summit sample, closer to the supply of colloidal Mn particles.

Very limited data is available on dissolved Te in the water column, comprising a single profile from each of the Pacific and Atlantic oceans (Yoon et al., 1990). According to this data, Te has a scavenged-type profile with ^{dis}Te content decreasing from 1 pM between 0–1000 mbsl to 0.74 pM between 1000–2000 and to 0.64 pM between 2000–3000 mbsl (Yoon et al., 1990). Although, modern-day species distribution might not reflect past ocean chemistry, the very similar Te concentrations, although lower by 5–10% in the flank sample, in both Tropic Seamount samples are consistent with this trend.

The behaviour of Pt in the water column cannot be generalised, with nutrient-like profiles observed in the Pacific Ocean, scavenger-type behaviour reported in the Indian Ocean, and both trends identified in the Atlantic Ocean (Jacinto and van den Berg, 1989; Colodoner, 1991; López-Sánchez et al., 2019). The observed differences between the ocean basins may be partly linked to differences in methods used to preconcentrate and detect Pt (López-Sánchez et al., 2019). Sources and sinks of Pt in seawater, the effect of its residence time and low reactivity on

its behaviour in the water column remain poorly constrained (López-Sánchez et al., 2019). However, it is notable that all reported seawater profiles show less than ±20% variation in the ^{dis}Pt content between depths of 1000–3000 mbsl, and the greatest variation occurs at the lower limit of the OMZ. Based on the profiles shown in Fig. 7, the Pt content is higher in the flank sample, suggesting a nutrient-type behaviour for Pt in the water around Tropic Seamount. Similarly, it is difficult to conclude on the general behaviour of Pt in seawater over the last 75 Ma based on modern-day measurements.

4.2. Pt and Te enrichments

Based on the samples studied from Tropic Seamount, Pt and Te have the highest enrichment factors of all the metals of economic interest in the older part of the deposit, and show no statistical association with Fe, Mn, Co, Ni and Cu (Supplementary material 1). Similar levels of PGE enrichment in old, phosphatised crusts have been reported (Halbach et al., 1989a; Hein et al., 2005; Asavin et al., 2010). A large body of leaching and precipitation experiments, phase association observations (XANES) and geochemical data suggest there are multiple mechanisms for Pt and Te incorporation into Fe-Mn oxides (Hein et al., 2003; Kashiwabara et al., 2014; Maeno et al., 2016; Koschinsky et al., 2020). These include sorption, redox processes and the phase transfer of the diverse species of Pt (Pt^0, Pt^{2+}, Pt^{4+}) and Te (Te^{4+}, Te^{6+}). As such, these elements can occur in different oxidation states, hosted by both Fe and Mn oxides, and as metallic particles derived from detrital contributions (cosmic spherules, volcanic aerosols, other detrital sources) (Halbach et al., 1989a). The diversity of potential processes, illustrates the challenge associated with identifying the principal controls on Pt and Te enrichment in Fe-Mn crusts.

The data from Tropic Seamount are supportive of an important role for redox processes in the incorporation of Pt and Te into Fe-Mn crusts. This is notably highlighted by the sympathetic stratigraphic profiles and positive correlation observed between Pt-Te and the Ce anomaly in the flank sample (078_019) ($R^2 > 0.4$) (Fig. 7 and supplementary material 1) (Koschinsky et al., 2020). Furthermore, enrichments in Pt and Te that are associated with well-defined stratigraphic intervals in both samples may be the result of increased cosmogenic contributions. A notable example is the significant enrichment in Te and Pt that occurs at the Paleocene-Eocene transition hiatus.

4.3. The effect of phosphatisation

Phosphatisation of Fe-Mn crusts and its effect on transition metal mobility has been discussed by a number of authors (Halbach and Puteanus, 1984; Halbach et al., 1989a, 1989b; Hein et al., 1993, 2000; Koschinsky and Halbach, 1995; Koschinsky et al., 1997; Koschinsky and Hein, 2003; Jiahua et al., 2005). Previous work highlights that partial dissolution and recrystallisation of Mn oxides during phosphatisation results in the decoupling of Co from Cu, Ni, and Zn through preferential incorporation

of these metals in the layer vacancy and structural defects of newly formed todorokite (Koschinsky et al., 1997; Bodeï et al., 2007). Bulk geochemical data which show lower Fe/Mn, Co/Ni, Co/Cu and Co/Zn ratios in the older, phosphatised parts of Fe-Mn crusts have been used to infer these complex mineralogical and structural changes. Pt and Te, that are highly enriched in Fe-Mn crusts relative to seawater and average lithospheric composition (Hein et al., 2003; Kashiwabara et al., 2014; Lusty et al., 2018), are considered to become more enriched in phosphatised parts of samples (Halbach et al., 1989a; Hein et al., 2005; Asavin et al., 2010; Koschinsky et al., 2020).

However, the data presented in this study show that these trends and anomalous enrichments also occur in unphosphatised samples that represent a similar depositional period to phosphatised samples from Tropic Seamount (Fig. 7). A more appropriate comparison should consequently be older versus younger Fe-Mn crusts, rather than phosphatised versus unphosphatised Fe-Mn crusts. If the last phosphatisation episode is considered to act as a marker between 'old' and 'young' Fe-Mn crust generations at Tropic Seamount, the Co/Ni, Co/Zn and Co/Cu ratios of the old (75–38 Ma) Fe-Mn crusts subsamples are consistently 29–38%, 23–36% and 52–57% lower than the younger (38–0 Ma) subsamples irrespective of the depth of formation and secondary diagenetic phosphatisation. Similarly, the significant difference in Pt and Te concentrations between the old and young Fe-Mn crust from Tropic Seamount, with stratigraphically well-defined Pt and Te-rich layer in both samples, is further evidence for an alternative control to phosphatisation for the enrichment of these elements.

Although todorokite has been detected in phosphatised Fe-Mn crusts from this region (Marino et al., 2017), the fact that the flank sample never experienced suboxic diagenetic conditions whilst presenting similar geochemical patterns to the phosphatised summit sample suggests that the partial recrystallisation and preferential metal accommodation hypothesis in todorokite does not account entirely for the metal enrichment observed in phosphatised Fe-Mn crust from Tropic Seamount. As proposed in previous research on Pt (Halbach and Puteanus, 1984; Halbach et al., 1989b; Koschinsky et al., 2020), the simplest explanation for the variable concentrations found in Fe-Mn crusts is changing metal flux to the ocean over time. The data presented here for Pt, but also Te, Co, Cu, Ni and Zn strongly supports this view. This evidence does not preclude an additional influence on metal concentrations from intense suboxic phosphatisation conditions, following partial dissolution and recrystallization as exemplified by previous research (Koschinsky et al., 1997). Such mineralogical changes are notably well understood in diagenetic polymetallic nodules and explain the compositional spectrum observed in these Fe-Mn concretions (Bodeï et al., 2007; Wegorzewski and Kuhn, 2014; Josso et al., 2017; Wegorzewski et al., 2020). A similar isocon analysis on phosphatised samples from the Pacific Ocean and comparison with deeper water unphosphatised samples would provide valuable new data to further investigate the control proposed here, and to distinguish between the effect of tem-

poral changes in metal flux and the influence of diagenetic remineralisation on the metal content of Fe-Mn crusts in the Pacific Ocean.

4.4. Changing metal fluxes

The chemical budget of the oceans is a function of the continuously evolving balance between inputs and outputs, controlled by long-term evolution of the climate and tectonic processes. During the Cenozoic, the climate changed from a greenhouse state to an icehouse climate, with CO_2 concentrations in the atmosphere decreasing and ice sheets forming at the poles (Zachos et al., 2001). This transition was partially driven by the reorganisation of global oceanic circulation. In that regard, Tropic Seamount is ideally located to have recorded the closure of the Tethys Ocean, the change from equatorial to poleward oceanic circulation with deep-water formation in the Southern Ocean primarily, followed by the onset of Northern Component Water in the Oligocene (Josso et al., 2020a). Fe-Mn crusts from Tropic Seamount also proved to be sensitive records of the Miocene cooling, aridification of North Africa, Northern Hemisphere Glaciation as well as variations of the weathering rates of nearby continental masses induced by astronomical parameters (Josso et al., 2020a; Josso et al., 2021). Throughout this major period of climate change, rates of weathering of the continental masses varied greatly, whilst the progressive opening of the north Atlantic and changing oceanic circulation modified the rate of hydrothermal activity and the influence of coastal and continental margin processes. This continuously evolving ocean geochemistry and geographic change is likely to have had a profound influence on the composition of contemporaneously forming Fe-Mn crusts throughout the global ocean (Josso et al., 2020b).

5. CONCLUSIONS

This study provides a comparison of accurately dated geochemical profiles for two Fe-Mn crusts recovered at 1100 and 3000 mbsl from Tropic Seamount. Preservation of the 75–28 Ma period of deposition in both samples allows to compare the geochemistry of contemporaneous Fe-Mn crusts layers and evaluate the effects of phosphatisation.

Paleo-reconstruction of Tropic Seamount subsidence and eustasy demonstrates the samples only moved within a narrow (300 m) depth window during their entire depositional history. Therefore, changes in water depth over time can be excluded as a significant influence on the variable metal content.

Isocon analysis permits a robust assessment of the metal mass differences between phosphatised and unphosphatised samples and indicates strong enrichment in Pt, Te, Cu, Ni, Zn in the older phosphatised section of the sample relative to its younger unphosphatised part. When mass changes resulting from CFA precipitation are accounted for, it is evident that no loss of Fe, Mn or Co occurred during suboxic CFA impregnation. Only As, Sb and W are depleted in the older phosphatised part of the deposit.

Comparison of geochemical profiles over time, indicates similar variations in the flank and summit samples, with high Pt, Te, Cu, Ni content in the 75–50 Ma part of the deposit. Major differences in metal content between the two samples reflect the primary availability of dissolved metals at different depths in the water column. Cobalt concentrations consistently increase up the stratigraphy, resulting in larger Co/Ni, Co/Cu and Co/Zn ratios in both samples. Well-defined stratigraphic intervals in both samples have 3–5-fold enrichments in Pt and Te concentrations. These observations in both the phosphatised summit sample and the contemporaneous, unphosphatised flank sample, does not support phosphatisation as being the primary control on the variable metal enrichment in Fe-Mn crusts at Tropic Seamount. Conversely, the data presented here suggests that these variations are likely the result of changing metal fluxes to the ocean during the Late Cretaceous and Cenozoic driven by long-term evolution of the ocean-climate system, partially overprinted by later phosphatisation episodes and dilution by CFA precipitation.

6. RESEARCH DATA

Research Data associated with this article can be accessed at https://doi.org/10.5285/a2a0347b-530a-4798-83d2-61eb3cce78fe.

Declaration of Competing Interest

The authors declare that they have no known competing financial interests or personal relationships that could have appeared to influence the work reported in this paper.

APPENDIX A. SUPPLEMENTARY MATERIAL

Supplementary data to this article can be found online at https://doi.org/10.1016/j.gca.2021.06.002.

REFERENCES

Asavin A. M., Kubrakova I. V., Mel'nikov M. E., Tyutyunnik O. A. and Chesalova E. I. (2010) Geochemical zoning in ferromanganese crusts of Ita-MaiTai guyot. *Geochemistry Int.* **48**, 423–445.

Bau M., Koschinsky A., Dulski P. and Hein J. R. (1996) Comparison of the partitioning behaviours of yttrium, rare earth elements, and titanium between hydrogenetic marine

ferromanganese crusts and seawater. *Geochim. Cosmochim. Acta* **60**, 1709–1725.

Benites M., Hein J. R., Mizell K., Blackburn T. and Jovane L. (2020) Genesis and Evolution of Ferromanganese Crusts from the Summit of Rio Grande Rise, Southwest Atlantic Ocean. *Minerals* **10**, 349.

Bodeï S., Manceau A., Geoffroy N., Baronnet A. and Buatier M. (2007) Formation of todorokite from vernadite in Ni-rich hemipelagic sediments. *Geochim. Cosmochim. Acta* **71**, 5698–5716.

Colodoner D. (1991) The Marine Geochemistry of Rhenium, Iridium and Platinum, Department of Earth, Atmospheric and Planetary Sciences. Massachussetts Institute of Technology, p. 269.

Crosby A. G. and McKenzie D. (2009) An analysis of young ocean depth, gravity and global residual topography. *Geophys. J. Int.* **178**, 1198–1219.

Dutkiewicz A., Müller R. D., O'Callaghan S. and Jónasson H. (2015) Census of seafloor sediments in the world's ocean. *Geology* **43**, 795–798.

Firdaus M. L., Mashio A. S., Obata H., McAlister J. A. and Orians K. J. (2018) Distribution of zirconium, hafnium, niobium and tantalum in the North Atlantic Ocean, northeastern Indian Ocean and its adjacent seas. *Deep Sea Res. Part I* **140**, 128–135.

Frank T. D. and Arthur M. A. (1999) Tectonic forcings of Maastrichtian ocean-climate evolution. *Paleoceanography* **14**, 103–117.

González F. J., Somoza L., Hein J. R., Medialdea T., León R., Urgorri V., Reyes J. and Martín-Rubí J. A. (2016) Phosphorites, Co-rich Mn nodules, and Fe-Mn crusts from Galicia Bank, NE Atlantic: reflections of Cenozoic tectonics and paleoceanography. *Geochem. Geophys. Geosyst.* **17**, 346–374.

Grant J. A. (1986) The isocon diagram: A simple solution to Gresens' equation for metasomatic alteration. *Econ. Geol.* **81**, 1976–1982.

Gresens R. L. (1967) Composition-volume relationship of metasomatism. *Chem. Geol.* **2**, 47–65.

Halbach P., Kriete C., Prause B. and Puteanus D. (1989a) Mechanisms to explain the platinum concentration in ferromanganese seamount crusts. *Chem. Geol.* **76**, 95–106.

Halbach P. and Puteanus D. (1984) The influence of the carbonate dissolution rate on the growth and composition of Co-rich ferromanganese crusts from Central Pacific seamount areas. *Earth Planet. Sci. Lett.* **68**, 73–87.

Halbach P., Sattler C. D., Teichmann F. and Wahsner M. (1989b) Cobalt-rich and platinum-bearing manganese crust deposits on seamounts: Nature, formation and metal potential. *Mar. Geol.* **69**, 25–54.

Haq B. U. (2014) Cretaceous eustasy revisited. *Global Planet. Change* **113**, 44–58.

Haq B. U., Hardenbol J. and Vail P. R. (1987) Chronology of fluctuating sea levels since the triassic. *Science* **235**, 1156–1167.

Hein J. R., Koschinsky A., Bau M., Manheim F. T., Kang J.-K. and Roberts L. (2000) Cobalt-rich ferromanganese crusts in the Pacific. In *Handbook Of Marine Minerals Deposit* (ed. D. S. Cronan). CRC Press, Boca Raton, Florida, pp. 239–279.

Hein J. R., Koschinsky A. and Halliday A. N. (2003) Global occurrence of tellurium-rich ferromanganese crusts and a model for the enrichment of tellurium. *Geochim. Cosmochim. Acta* **67**, 1117–1127.

Hein J. R., Koschinsky A. and McIntyre B. (2005) The global enrichment of platinum group elements in marine ferromanganese crusts. In *Extended Abstracts, 10th International Platinum Symposium, 7–11 August 2005, Oulu, Finland* (eds. T. O. Törmänen and T. T. Alapieti).

Hein J. R., Koschinsky A., Mikesell M., Mizell K., Glenn C. R. and Wood R. (2016) Marine phosphorites as potential resources for heavy rare earth elements and yttrium. *Minerals* **6**, 88.

Hein J. R., Mizell K., Koschinsky A. and Conrad T. A. (2013) Deep-ocean mineral deposits as a source of critical metals for high- and green-technology applications: comparison with land-based resources. *Ore Geol. Rev.* **51**, 1–14.

Hein J. R., Yeh H.-W., Gunn S. H., Sliter W. V., Benninger L. M. and Wang C.-H. (1993) Two major cenozoic episodes of phosphogenesis recorded in equatorial pacific seamount deposits. *Paleoceanography* **8**, 293–311.

Humphris S. E., Alt J. C., Teagle D. A. H. and Honnorez J. J. (1998) Geochemical changes during hydrothermal alteration of basement in the stockwork beneath the active TAG hydrothermal mound. In Proceedings of the Ocean Drilling Program, Scientific Results (eds. P. M. Herzig, S. E. Humphris, D. J. Miller, & R. A. Zierenberg (Eds.)).

Jacinto G. S. and van den Berg C. M. G. (1989) Different behaviour of platinum in the Indian and Pacific Oceans. *Nature* **338**.

Jeong K. S., Jung H. S., Kang J. K., Morgan C. L. and Hein J. R. (2000) Formation of ferromanganese crusts on northwest intertropical Pacific seamounts: electron photomicrography and microprobe chemistry. *Mar. Geol.* **162**, 541–559.

Jiahua P., De Carlo E. H., Yi Y., Shuqin L. and Guoqin Y. (2005) Effect of phosphatization on element concentration of cobalt-rich ferromanganese crusts. *Acta Geol. Sin. - English Ed.* **79**, 349–355.

Jochum K. P., Nohl U., Herwig K., Lammel E., Stoll B. and Hofmann A. W. (2005) GeoReM: A new geochemical database for reference materials and isotopic standards. *Geostand. Geoanal. Res.* **29**, 333–338.

Josso P., Horstwood M. S. A., Millar I. L., Pashley V., Lusty P. A. J. and Murton B. (2020a) Development of a correlated Fe-Mn crust stratigraphy using Pb and Nd isotopes and its application to paleoceanographic reconstruction in the Atlantic. *Paleoceanogr. Paleoclimatol.* **35**, e2020PA003928.

Josso P., Parkinson I., Horstwood M., Lusty P., Chenery S. and Murton B. (2019) Improving confidence in ferromanganese crust age models: a composite geochemical approach. *Chem. Geol.* **513**, 108–119.

Josso P., Pelleter E., Pourret O., Fouquet Y., Etoubleau J., Cheron S. and Bollinger C. (2017) A new discrimination scheme for oceanic ferromanganese deposits using high field strength and rare earth elements. *Ore Geol. Rev.* **87**, 3–15.

Josso P., Rushton J., Lusty P., Matthews A., Chenery S., Holwell D., Kemp S. J. and Murton B. (2020b) Late Cretaceous and Cenozoic paleoceanography from north-east Atlantic ferromanganese crust microstratigraphy. *Mar. Geol.* **422** 106122.

Josso P., van Peer T., Horstwood M. S. A., Lusty P. and Murton B. (2021) Geochemical evidence of Milankovitch cycles in Atlantic Ocean ferromanganese crusts. *Earth Planet. Sci. Lett.* **553** 116651.

Kashiwabara T., Oishi Y., Sakaguchi A., Sugiyama T., Usui A. and Takahashi Y. (2014) Chemical processes for the extreme enrichment of tellurium into marine ferromanganese oxides. *Geochim. Cosmochim. Acta* **131**, 150–163.

Koschinsky A. and Halbach P. (1995) Sequential leaching of marine ferromanganese precipitates: Genetic implications. *Geochim. Cosmochim. Acta* **59**, 5113–5132.

Koschinsky A., Halbach P., Hein J. R. and Mangini A. (1996) Ferromanganese crusts as indicators for paleoceanographic events in the NE Atlantic. *Geol. Rundsch.* **85**, 567–576.

Koschinsky A. and Hein J. R. (2003) Uptake of elements from seawater by ferromanganese crusts: solid-phase associations and seawater speciation. *Mar. Geol.* **198**, 331–351.

Koschinsky A., Hein J. R., Kraemer D., Foster A. L., Kuhn T. and Halbach P. (2020) Platinum enrichment and phase associations in marine ferromanganese crusts and nodules based on a multi-method approach. *Chem. Geol.* **539** 119426.

Koschinsky A., Stascheit A., Bau M. and Halbach P. (1997) Effects of phosphatization on the geochemical and mineralogical composition of marine ferromanganese crusts. *Geochim. Cosmochim. Acta* **61**, 4079–4094.

López-Sánchez D. E., Cobelo-García A., Rijkenberg M. J. A., Gerringa L. J. A. and de Baar H. J. W. (2019) New insights on the dissolved platinum behavior in the Atlantic Ocean. *Chem. Geol.* **511**, 204–211.

Lusty P., Hein J. R. and Josso P. (2018) Formation and occurence of ferromanganese crusts: Earth's storehouse for critical metals. *Elements* **14**, 313–318.

Maeno M. Y., Ohashi H., Yonezu K., Miyazaki A., Okaue Y., Watanabe K., Ishida T., Tokunaga M. and Yokoyama T. (2016) Sorption behavior of the Pt(II) complex anion on manganese dioxide (δ-MnO$_2$): a model reaction to elucidate the mechanism by which Pt is concentrated into a marine ferromanganese crust. *Miner. Deposita* **51**, 211–218.

Marino E., González F. J., Somoza L., Lunar R., Ortega L., Vázquez J. T., Reyes J. and Bellido E. (2017) Strategic and rare elements in Cretaceous-Cenozoic cobalt-rich ferromanganese crusts from seamounts in the Canary Island Seamount Province (northeastern tropical Atlantic). *Ore Geol. Rev.* **87**, 41–61.

Mizell K., Hein J. R., Koschinsky A. and Hayes S. M. (2020a) Effects of phosphatization on the mineral associations and speciation of Pb in ferromanganese crusts. *ACS Earth Space Chem.*.

Mizell K., Hein J. R., Lam P. J., Koppers A. A. P. and Staudigel H. (2020b) Geographic and oceanographic influences on ferromanganese crust composition along a Pacific Ocean Meridional Transect, 14 N to 14S. *Geochem. Geophys. Geosyst.* **21**, e2019GC008716.

Muiños S. B., Hein J. R., Frank M., Monteiro J. H., Gaspar L., Conrad T., Pereira G. and Abrantes F. (2013) Deep-sea Fe-Mn crusts from the northeast Atlantic Ocean: composition and resource considerations. *Mar. Georesour. Geotechnol.* **31**, 40–70.

Oldham V. E., Jones M. R., Tebo B. M. and Luther G. W. (2017) Oxidative and reductive processes contributing to manganese cycling at oxic-anoxic interfaces. *Mar. Chem.* **195**, 122–128.

Schlitzer R., Anderson R. F., Dodas E. M., Lohan M., Geibert W., Tagliabue A., Bowie A., Jeandel C., Maldonado M. T., Landing W. M., Cockwell D., Abadie C., Abouchami W., Achterberg E. P., Agather A., Aguilar-Islas A., van Aken H. M., Andersen M., Archer C., Auro M., de Baar H. J., Baars O., Baker A. R., Bakker K., Basak C., Baskaran M., Bates N. R., Bauch D., van Beek P., Behrens M. K., Black E., Bluhm K., Bopp L., Bouman H., Bowman K., Bown J., Boyd P., Boye M., Boyle E. A., Branellec P., Bridgestock L., Brissebrat G., Browning T., Bruland K. W., Brumsack H.-J., Brzezinski M., Buck C. S., Buck K. N., Buesseler K., Bull A., Butler E., Cai P., Mor P. C., Cardinal D., Carlson C., Carrasco G., Casacuberta N., Casciotti K. L., Castrillejo M., Chamizo E., Chance R., Charette M. A., Chaves J. E., Cheng H., Chever F., Christl M., Church T. M., Closset I., Colman A., Conway T. M., Cossa D., Croot P., Cullen J. T., Cutter G. A., Daniels C., Dehairs F., Deng F., Dieu H. T., Duggan B., Dulaquais G., Dumousseaud C., Echegoyen-Sanz Y., Edwards R. L., Ellwood M., Fahrbach E., Fitzsimmons J. N., Russell Flegal A., Fleisher M. Q., van de Flierdt T., Frank M., Friedrich J., Fripiat F., Fröllje H., Galer S. J. G., Gamo T., Ganeshram R. S., Garcia-Orellana J.,

Garcia-Solsona L. J. A., Gault-Ringold M., George E., Gerringa L. J. A., Gilbert M., Godoy J. M., Goldstein S. L., Gonzalez S. R., Grissom K., Hammerschmidt C., Hartman A., Hassler C. S., Hathorne E. C., Hatta M., Hawco N., Hayes C. T., Heimbürger L.-E., Helgoe J., Heller M., Henderson G. M., Henderson P. B., van Heuven S., Ho P., Horner T. J., Hsieh Y.-T., Huang K.-F., Humphreys M. P., Isshiki K., Jacquot J. E., Janssen D. J., Jenkins W. J., John S., Jones E. M., Jones J. L., Kadko D. C., Kayser R., Kenna T. C., Khondoker R., Kim T., Kipp L., Klar J. K., Klunder M., Kretschmer S., Kumamoto Y., Laan P., Labatut M., Lacan F., Lam P. J., Lambelet M., Lamborg C. H., Le Moigne F. A. C., Le Roy E., Lechtenfeld O. J., Lee J.-M., Lherminier P., Little S., López-Lora M., Lu Y., Masque P., Mawji E., McClain C. R., Measures C., Mehic S., Barraqueta J.-L. M., van der Merwe P., Middag R., Mieruch S., Milne A., Minami T., Moffett J. W., Moncoiffe G., Moore W. S., Morris P. J., Morton P. L., Nakaguchi Y., Nakayama N., Niedermiller J., Nishioka J., Nishiuchi A., Noble A., Obata H., Ober S., Ohnemus D. C., van Ooijen J., O'Sullivan J., Owens S., Pahnke K., Paul M., Pavia F., Pena L. D., Peters B., Planchon F., Planquette H., Pradoux C., Puigcorbé V., Quay P., Queroue F., Radic A., Rauschenberg S., Rehkämper M., Rember R., Remenyi T., Resing J. A., Rickli J., Rigaud S., Rijkenberg M. J. A., Rintoul S., Robinson L. F., Roca-Martí M., Rodellas V., Roeske T., Rolison J. M., Rosenberg M., Roshan S., Rutgers van der Loeff M. M., Ryabenko E., Saito M. A., Salt L. A., Sanial V., Sarthou G., Schallenberg C., Schauer U., Scher H., Schlosser C., Schnetger B., Scott P., Sedwick P. N., Semiletov I., Shelley R., Sherrell R. M., Shiller A. M., Sigman D. M., Singh S. K., Slagter H. A., Slater E., Smethie W. M., Snaith H., Sohrin Y., Sohst B., Sonke J. E., Speich S., Steinfeldt R., Stewart G., Stichel T., Stirling C. H., Stutsman J., Swarr G. J., Swift J. H., Thomas A., Thorne K., Till C. P., Till R., Townsend A. T., Townsend E., Tuerena R., Twining B. S., Vance D., Velazquez S., Venchiarutti C., Villa-Alfageme M., Vivancos S. M., Voelker A. H. L., Wake B., Warner M. J., Watson R., van Weerlee E., Alexandra Weigand M., Weinstein Y., Weiss D., Wisotzki A., Woodward E. M. S., Wu J., Wu Y., Wuttig K., Wyatt N., Xiang Y., Xie R. C., Xue Z., Yoshikawa H., Zhang J., Zhang P., Zhao Y., Zheng L., Zheng X.-Y., Zieringer M., Zimmer L. A., Ziveri P., Zunino P. and Zurbrick C. (2018) The GEOTRACES Intermediate Data Product 2017. *Chem. Geol.* **493**, 210–223.

Taylor S. R. and McLennan S. M. (1985) The continental Crust: Its composition and Evolution. Blackwell Scientific, Boston, Mass., 312 p.

Tripati A., Backman J., Elderfield H. and Ferretti P. (2005) Eocene bipolar glaciation associated with global carbon cycle changes. *Nature* **436**, 341–346.

Watts A. B. and Zhong S. (2000) Observations of flexure and the rheology of oceanic liithosphere. *Geophys. J. Int.* **142**, 855–875.

Wegorzewski A. V., Grangeon S., Webb S. M., Heller C. and Kuhn T. (2020) Mineralogical transformations in polymetallic nodules and the change of Ni, Cu and Co crystal-chemistry upon burial in sediments. *Geochim. Cosmochim. Acta*.

Wegorzewski A. V. and Kuhn T. (2014) The influence of suboxic diagenesis on the formation of manganese nodules in the Clarion Clipperton nodule belt of the Pacific Ocean. *Mar. Geol.*.

Yeo I., Dobson K., Josso P., Pearce R., Howarth S., Lusty P., Le Bas T. and Murton B. (2018) Assessment of the mineral resource potential of Atlantic ferromanganese crusts based on their growth history, microstructure, and texture. *Minerals* **8**, 327.

Yeo I. A., Howarth S. A., Spearman J., Cooper A., Crossouard N., Taylor J., Turnbull M. and Murton B. J. (2019) Distribution of

and hydrographic controls on ferromanganese crusts: tropic Seamount, Atlantic. *Ore Geol. Rev.* **114** 103131.

Yoon B. M., Shim S. C., Pyun H. C. and Lee D. S. (1990) Hydride generation atomic absorption determination of tellurium species in environmental samples with *in Situ* concentration in a graphite furnace. *Anal. Sci.* **6**, 561–566.

Zachos J., Pagani M., Sloan L., Thomas E. and Billups K. (2001) Trends, rhythms, and aberrations in global climate 65 Ma to present. *Science* **292**, 686–693.

Associate editor: Caroline P. Slomp